ADVANCED MATERIALS TECHNOLOGIES
www.advmattechnol.de

Unobtrusive Swallow Monitoring Enabled by Conformal IONOGEL Biopotential Electrodes and Machine Learning

*Penghao Dong, Jasmine Ives, Ethan Garcia, Christopher Caporusso, Polina Bragina, Cassandra Laguatan, and Shanshan Yao**

Dysphagia or difficulty swallowing is caused by the failure of neurological pathways to properly activate swallowing muscles. Current electromyography (EMG) systems for dysphagia monitoring are bulky and rigid, limiting their potential for long-term and unobtrusive use. To address this, a machine learning-assisted wearable EMG system is presented, utilizing self-adhesive, skin-conformal, semi-transparent, and robust ionic gel electrodes. The presented electrodes possess good conductivity, superior skin contact, and good transmittance, ensuring high-fidelity EMG sensing without impeding daily activities. Moreover, the optimized material and structural designs ensure wearing comfort and conformable skin-electrode contact, allowing for long-term monitoring with high accuracy. Machine learning and mel-frequency cepstral coefficient techniques are employed to classify swallowing events based on food types and volumes. Through an analysis of electrode placement on the chin and neck, the proposed system is able to effectively distinguish between different food types and water volumes using a small number of channels, making it suitable for continuous dysphagia monitoring. This work represents an advancement in machine learning assisted EMG systems for the classification and regression of swallowing events, paving the way for more efficient, unobtrusive, and long-term dysphagia monitoring systems.

1. Introduction

The swallowing process involves a complex coordination of over 50 pairs of muscles and both voluntary and involuntary neurologic pathways. Dysphagia or difficulty swallowing arises when neurological pathways fail to properly activate swallowing muscles.[1] If left untreated, dysphagia can lead to severe complications such as choking, nasal regurgitation, dehydration, malnutrition, aspiration pneumonia, and even death.[2–5] Additionally, dysphagia can have significant psychological effects, including reduced self-esteem, embarrassment, and social anxiety among patients.[6]

Effective rehabilitation for dysphagia typically involves biofeedback techniques, muscle-strengthening exercises, and dietary modifications aimed at improving swallowing efficiency. However, adherence to these treatments remains low, with studies indicating that only 22% to 52% of patients complete their rehabilitation programs.[7] A significant reason for this low adherence is the cumbersome and expensive nature of traditional biofeedback devices. For instance, the gold standard for diagnosing dysphagia is the videofluoroscopic swallow study (VFSS), which provides valuable insights into the swallowing process.[8] However, VFSS has several limitations, including requiring an X-ray machine, exposing patients to ionizing radiation, and potential side effects from barium contrast.[9] Moreover, there is an increasing need for portable and easy-to-use devices that can screen for early-stage swallowing disorders.[10] Detecting these problems early is vital for preventing dysphagia from worsening.

To fill in these gaps, new devices based on electromyogram (EMG)[11–13] or inertial measurement units (IMUs)[14,15] have been developed to monitor swallowing-induced bio-signals continuously. EMG has become an essential tool due to its effectiveness in detecting and diagnosing dysphagia by monitoring complex muscle activities involved in swallowing.[16–18] However, most commercially available EMG devices rely on pre-gelled Ag/AgCl electrodes. While effective, gel electrodes can trigger skin irritations and become unreliable for long-term use as the gel dries out.[19–21] To address this issue, soft electrodes are developed for dysphagia diagnosis. Table S1 (Supporting Information) details the comparison between current research efforts on soft wearable devices for swallowing monitoring. These sensors or electrodes, placed under the chin or on the neck, allow for continuous monitoring of swallowing behaviors.[12,13] Related studies have demonstrated the feasibility of such sensor patches, which are typically outfitted with metal electrodes on an elastomeric substrate.[12] Metal EMG electrodes, as dry electrodes, offer

P. Dong, J. Ives, C. Caporusso, P. Bragina, C. Laguatan, S. Yao
Department of Mechanical Engineering
Stony Brook University
Stony Brook, NY 11794, USA
E-mail: shanshan.yao@stonybrook.edu
E. Garcia
Department of Electrical and Computer Engineering
Stony Brook University
Stony Brook, NY 11794, USA

The ORCID identification number(s) for the author(s) of this article can be found under https://doi.org/10.1002/admt.202500229

DOI: 10.1002/admt.202500229

superior biocompatibility and excellent conductivity, though they may face challenges in terms of durability, skin-electrode contact, and signal stability due to the mechanical mismatch between the electrode and the skin.[22] Moreover, their opacity and invasive appearance may discourage long-term use. Additionally, the methods for analyzing EMG signals collected by these sensors are still under development, limiting their ability to provide detailed feedback on specific muscle performance during swallowing.[23]

Conductive polymers, including hydrogels and ionic gels, have emerged as potential electrodes for swallow monitoring.[24] Hydrogels stand out for their softness and ability to adhere to biological tissues. These materials can be tuned to achieve desirable mechanical, electrical, and chemical properties, making them suitable for wearable electronics.[25] However, hydrogels have limitations in non-aqueous environments due to their tendency to dehydrate.[26] Ionic gels, which combine ionic liquids with polymer matrices, offer high conductivity, transparency, and stability. These materials are particularly attractive for wearable devices due to their negligible vapor pressure and thermal stability.[27]

Machine learning techniques, such as Support Vector Machines (SVMs) and Artificial Neural Networks (ANNs), are widely used in health monitoring, including bio-signal analysis.[28–31] SVM is robust to overfitting, especially in high-dimensional spaces and for small datasets.[32,33] In applications that involve limited training samples, for instance, EEG-based systems for detecting physiological artifacts (e.g., eye blinks)[30] and EMG-driven prosthetics for movement classification,[31] SVM outperforms ANN because SVM is able to generalize with minimal data, whereas ANN is dependent on extensive datasets to avoid overfitting. On the other hand, ANN's structure enables automatic feature learning and modeling of complex non-linear relationships, although it typically requires a careful hyperparameter tuning process and large datasets to avoid overfitting.[34] This distinction highlights the advantage of SVMs in resource-constrained bio-signal applications, where data acquisition is inherently limited.

This work presents an EMG-based monitoring system based on adhesive, skin-conformal, unobtrusive ionic gel electrodes and machine learning. This system aims to address the above challenges through innovations in materials, sensing locations, and signal processing algorithms. This article presents improvements in 1) enhancing electrode unobtrusiveness and skin-electrode contact for improved signal quality, long-term use, and wearing comfort; and 2) developing datasets corresponding to food categories and machine learning algorithms to enhance the electrode's ability to detect various swallowing maneuvers. The study begins with an overview of the EMG-based swallow monitoring process, followed by a detailed exploration of the electrode's design, fabrication, and performance evaluation. Particularly, the designed electrode achieves great conductivity, adhesiveness, transmittance, stability, as well as excellent sensing performance. As for the signals relevant to swallowing processes, machine learning algorithms and segmentation methods are employed to analyze them to optimize electrode placement along a subject's chin and neck for precise detection of swallowing events. The detailed analysis demonstrates the proposed system's exceptional ability to classify different types of swallows based on different types of food as well as to predict water volumes via regression. The key advantage of this design lies in the IONOGEL electrodes' superior skin conformity, flexibility, transparency, and signal fidelity, which enables unobtrusive and continuous monitoring of swallowing with great wearing comfort. Combined with robust machine learning models, this system represents a highly efficient and reliable tool for both clinical and real-world rehabilitation applications, offering seamless and non-invasive tracking of swallowing dynamics.

2. Result and Discussion

2.1. Overview of the EMG-Based Swallow Monitoring Process

Figure 1 presents the architecture of the EMG-based swallow monitoring system, which integrates the epidermal ionic gel (IONOGEL) EMG sensing electrodes with machine learning-based classification and regression algorithms. Utilizing the bipolar configuration[35] for EMG sensing, five pairs of skin-conformal IONOGEL electrodes are strategically placed on the chin and neck skin, forming five sensing channels to capture high-fidelity muscular activities during swallowing (Figure 1a). A shared ground electrode is positioned on the clavicle, a low-activity muscle area, to reduce noise interference and enhance signal stability.

After the data collection, essential pre-processing techniques are applied to the collected EMG signals. A bandpass filter and a notch filter (Figure 1b) are necessary to reduce noise caused by motion artifacts[36] and to eliminate power line interference.[37] Once clean signals are obtained, they are segmented so that each segment corresponds to a single swallow. This segmentation allows for precise feature extraction from each swallowing event, producing matrices for downstream analysis. Further preprocessing details are discussed in Section 2.3. Then, the feature matrices are processed by a fully connected artificial neural network (ANN) and a support vector machine (SVM) model, optimizing both training and channel selection (Figure 1c). The model delivers highly accurate classifications of food categories and precise regressions for predicting swallowed water volumes (Figure 1d). The integration of machine learning enhances the system's ability to provide insights into the swallowing process, as detailed in Section 2.4.

2.2. Optimization and Performance of the Electrode

The IONOGEL electrode is innovatively designed using a combination of 1-Ethyl-3-methylimidazolium bis(trifluoromethylsulfonyl)imide (EMIM TFSI), waterborne polyurethane (WPU), and poly(3,4-ethylenedioxythiophene)-poly(styrenesulfonate) (PEDOT:PSS), each contributing to its exceptional performance (**Figure 2a**). EMIM TFSI, an ionic liquid, ensures efficient ion transport while helping the electrode maintain a high degree of softness and adhesion, which is critical for seamless skin integration. WPU, a water-based polyurethane, adds superior stretchability and mechanical compliance,[38] making the electrode highly adaptable to the natural movements of the skin. PEDOT:PSS, a conductive polymer, enhances electrical

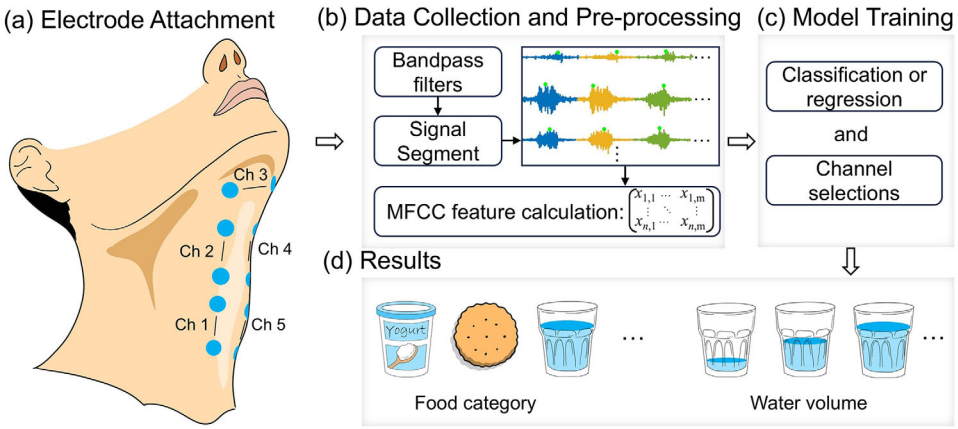

Figure 1. Overview of the EMG-based swallow monitoring process. a) Schematics showing the electrode position on the neck. b) EMG data acquisition and pre-processing. c) Machine learning model training and channel selection. d) Classification results of the food category and regression results of the water volume.

conductivity, ensuring reliable sensing performance of the electrodes. The fabrication process, which involves stirring these components into a homogeneous solution, drop-casting onto a glass substrate, and knife cutting, allows for precise electrode design (Figure 2b–d). Once patterned, the electrodes can be easily peeled off and applied directly to the skin (Figure 2e,f), offering an efficient and skin-friendly interface for EMG sensing that combines comfort, durability, visual unobtrusiveness, and high sensing performance.

To optimize and evaluate the electrode design, the mechanical, electrical, optical, and sensing performances were characterized via a series of experiments. By varying the weight ratios of WPU, EMIM TFSI, and PEDOT:PSS, an optimized material composition was achieved that produces an electrode with high conductivity, mechanical compliance, transmittance, and skin adhesion. Additionally, with the help of acquired mechanical properties and an energy-based analytical model, the electrode was optimized to achieve conformal contact with the skin for improved signal quality and wearing comfort.

For an EMIM TFSI loading in WPU beyond 50 wt.%, the resulting electrode is unstable and cannot form a self-standing thin film. Thus, the weight ratio between the EMIM TFSI and WPU

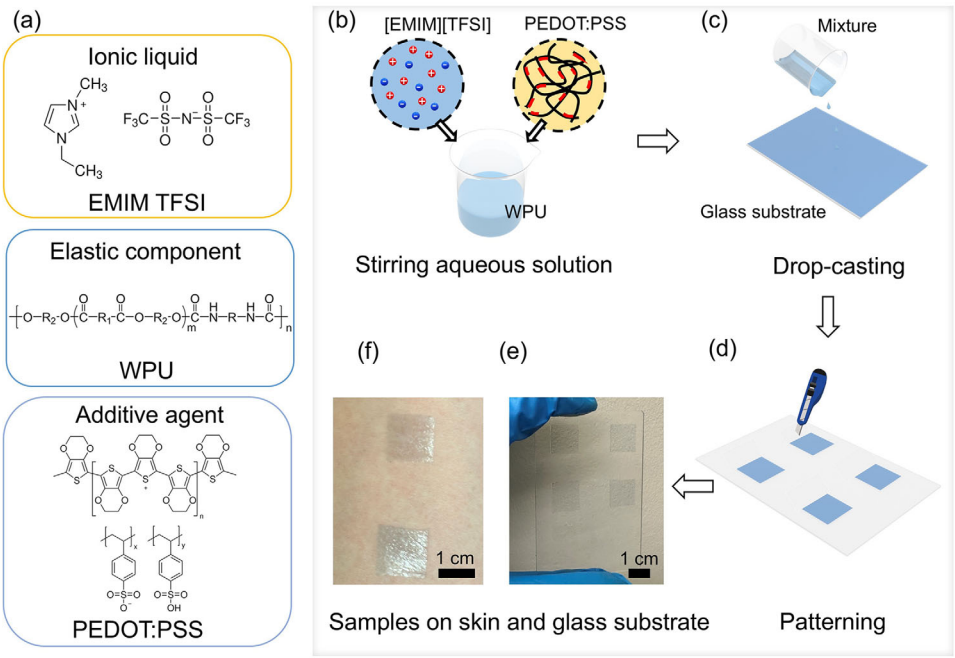

Figure 2. Fabrication process of the IONOGEL electrode. a) Chemical structures of PEDOT:PSS, EMIM TFSI, and WPU. b) Stirring process to obtain the solution of all materials. c) Drop casting of the solution into a thin film. d) Patterning of the final IONOGEL electrode using a utility knife. Each electrode is in the shape of a 13 mm square. e) Pictures of a set of fabricated IONOGEL electrodes on the glass substrate. f) Picture of one pair of IONOGEL electrodes attached to the skin. The electrodes shown are IONOGEL-30 2% PEDOT.

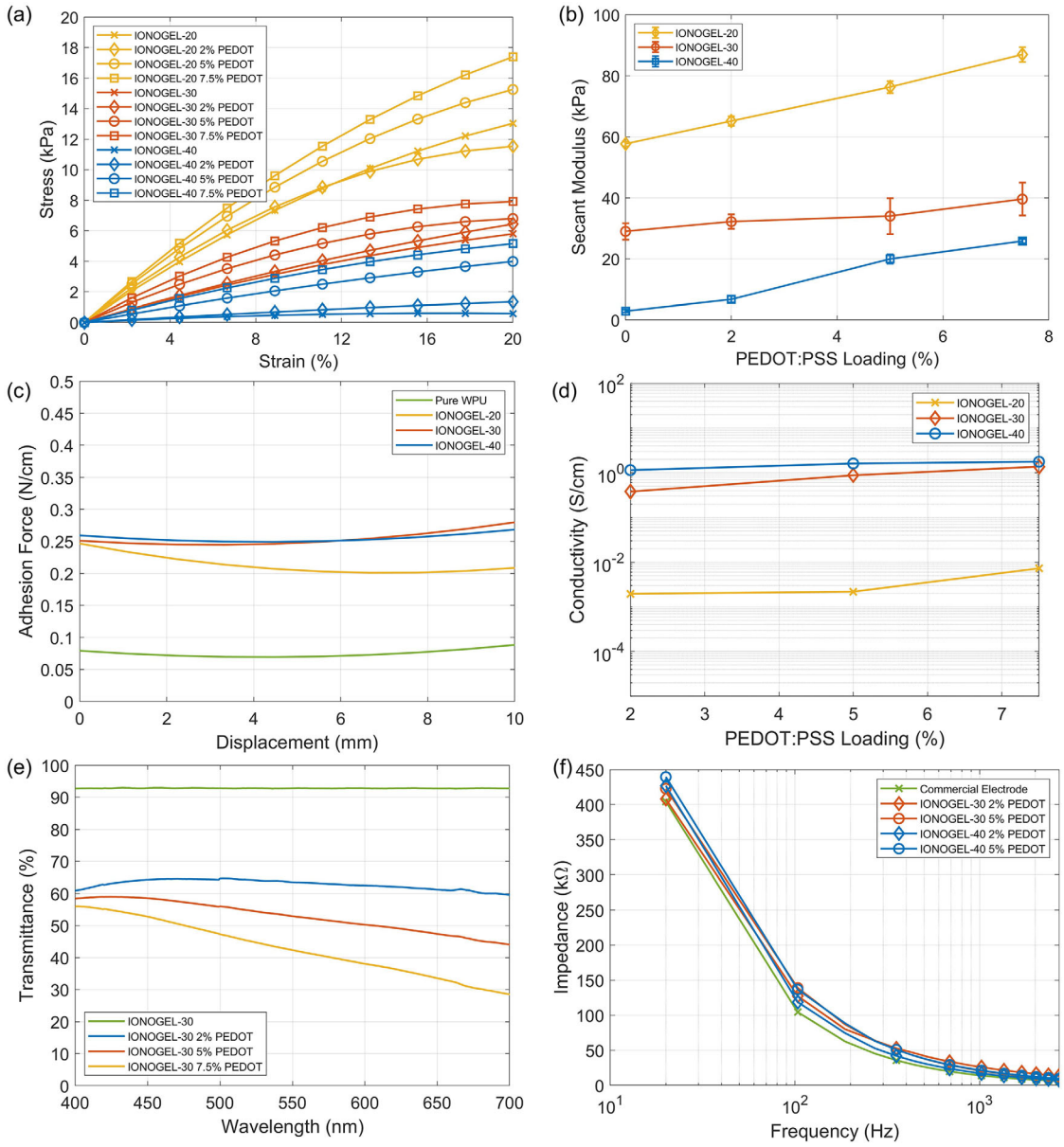

Figure 3. Characterizations of IONOGEL electrodes with different material compositions. a) Stress–strain curves of IONOGEL electrodes. b) Comparisons of secant moduli of IONOGEL with different composition ratios. The secant modulus is the slope drawn from the origin of the stress–strain curve and intersecting the curve at the point of interest, which in this case is at 20% strain. c–f) Comparisons of c) adhesion force, d) conductivity, e) transmittance, and f) electrode-skin impedance for IONOGEL electrodes with different composition ratios.

was set to 2:8, 3:7, and 4:6 for experiments. Meanwhile, increasing PEDOT:PSS amount will significantly decrease the transmittance. The weight ratios of PEDOT:PSS were set to 2%, 5%, and 7.5%, respectively. One example of denotation is IONOGEL-20 2% PEDOT, which means the weight ratio between the ionic liquid and WPU is 2:8, and the weight ratio of PEDOT:PSS is 2% of the total mixture weight.

Figure 3a,b compares the stress–strain behaviors and corresponding secant moduli at different WPU, EMIM TFSI, and PEDOT:PSS ratios, while Figure 3c shows the electrode adhesion tested on the pig skin. The electrode shows nonlinear elasticity due to the properties of WPU. As the ratio of ionic liquid to WPU increases, the material becomes softer, and the adhesion force increases. It should be noted that the adhesion force of IONOGEL-30 to IONOGEL-40 is similar (Figure 3c). A softer material with a higher adhesion force is more conducive to high-fidelity EMG signals as it can help achieve conformal contact and thus low electrode-skin impedance. To quantitatively evaluate the conformal contact of electrodes with different material compositions, an energy-based analytical model (detailed in Note S1, Supporting Information) was used. The model was modified from our previous work[39] to adapt to the nonlinear elasticity. As shown in Table S3 (Supporting Information), the critical thickness of the IONOGEL electrodes, which means the electrode must be below

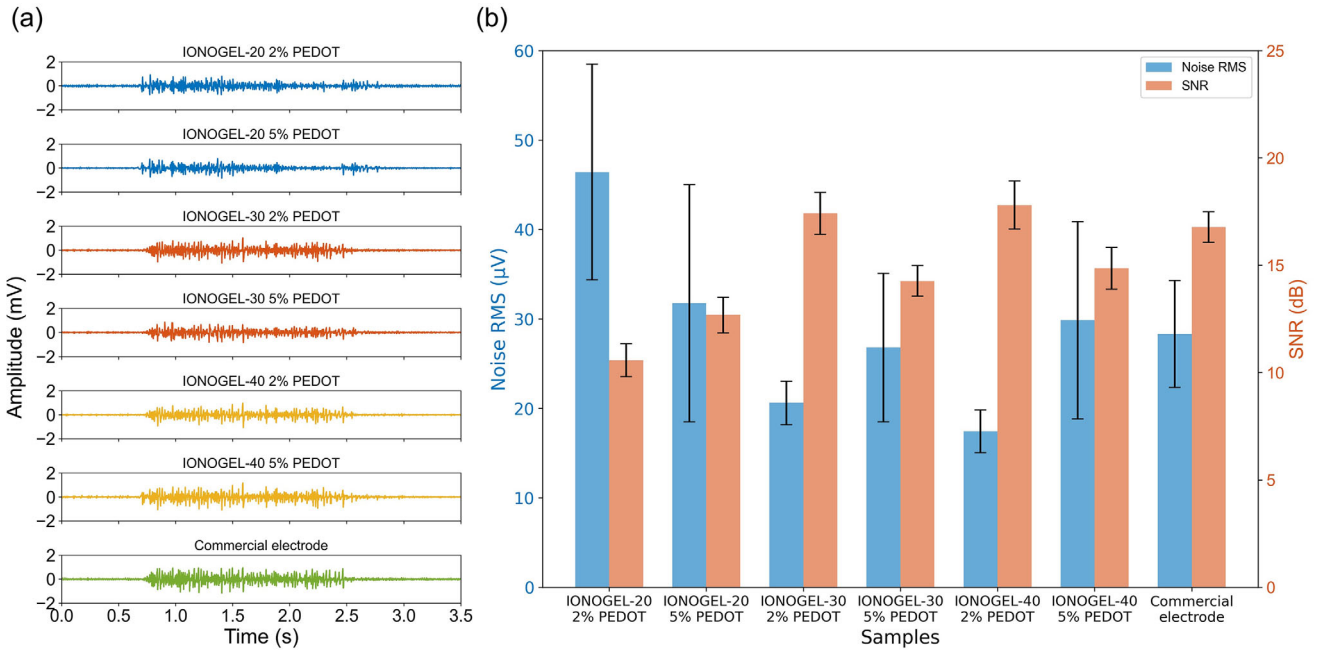

Figure 4. Signal comparisons for different electrodes. Comparisons of a) EMG signals and b) SNR and noise RMS for IONOGEL electrodes with different compositions and the commercial electrode.

this threshold to achieve conformal contact with the skin, varies from 23 to 75 μm when increasing the weight ratio of ionic liquid in WPU. Typically, a larger critical thickness means it is easier to fabricate an electrode that can achieve conformal contact. As the amount of ionic liquid increases from 20 wt.% in IONOGEL-20 to 30 wt.% in IONOGEL-30, the critical thickness jumps from 23 to 60 μm. IONOGEL-40 has a larger critical thickness, which is 75 μm, compared to IONOGEL-30 but the improvement is relatively smaller than the improvement of IONOGEL-30 to IONOGEL-20. The addition of PEDOT:PSS within the IONOGEL matrix has an increasing effect on the secant modulus of the material for a loading ratio of 0–7.5 wt.% (Figure 3b). Based on the modulus, adhesion force, and conformal contact analysis, IONOGEL-30 and IONOGEL-40 are better than IONOGEL-20 for the electrode.

Figure S2 (Supporting Information) illustrates that increasing the ratio of ionic liquid to WPU can effectively improve the conductivity. With the PEDOT:PSS added in, the conductivity of IONOGEL is further enhanced (Figure 3d; Figure S2, Supporting Information). This is owing to PEDOT:PSS's favorable ion exchange capability with the ionic liquid and PEDOT:PSS's electrical conductivity.[40–42] Even the PEDOT:PSS can enhance the conductivity, it also lowers the transmittance of the electrode (Figure 3e). Taking IONOGEL-30 as an example, with a 7.5% PEDOT:PSS add-in, the transmittance under most wavelengths is below 50%. Since the loading of PEDOT:PSS equal to or larger than 7.5 wt.% results in an undesirable transmittance and a minor conductivity improvement, 2 and 5 wt.% loading of PEDOT:PSS was chosen for further studies and analysis.

The impedance analysis shows several selected samples have comparable performance to the commercial gel electrode (Figure 3f). **Figure 4a** compares the signals of IONOGEL electrodes against the commercial Ag/AgCl electrodes. Figure 4b shows that IONOGEL-20 electrodes containing 2% PEDOT or 5% PEDOT were unable to collect high-fidelity signals, showing lower signal-to-noise ratio (SNR) and high noise root mean square (RMS) compared to other samples or commercial electrodes. IONOGEL-30 and IONOGEL-40 samples performed comparably to the commercial electrode in both RMS and SNR. The conformal contact and high conductivity of these IONOGEL electrodes guarantee high signal quality and low noise of the electrode. For the detection of swallowing events that involve small voluntary and involuntary infrahyoid and suprahyoid muscle groups, low noise RMS and high SNRs are essential for accurate data collection and classification of signals. Among all samples, IONOGEL-40 2% PEDOT and IONOGEL-30 2% PEDOT demonstrate better performance due to their superior softness, which enhances skin conformity, and their high content of EMIM TFSI and PEDOT:PSS, facilitating efficient signal transduction. However, IONOGEL-40's extreme softness makes it challenging to maintain a freestanding structure during experiments, hindering its application on human skin. For practical use, IONOGEL-30 2% PEDOT was selected as the electrode material because it offers a good balance of performance, structural stability, and transmittance.

The wearing comfort of IONOGEL-30 with 2% PEDOT was further analytically calculated (Note S2, Supporting Information). The maximum normal stress generated from the electrode is calculated to be 29.1 kPa (more details in Note S2, Supporting Information), lower than the pressure threshold (60–170 kPa) that causes discomfort for the chin and neck skin (areas of interest).[43] Further, none of the subjects reported noticeable pressure from the electrodes or skin discomfort during data acquisition, confirming the electrodes' good wearing comfort. The resistance-strain performance for the IONOGEL-30 with 2% PEDOT:PSS was also tested. When subjected to around 15% strain,

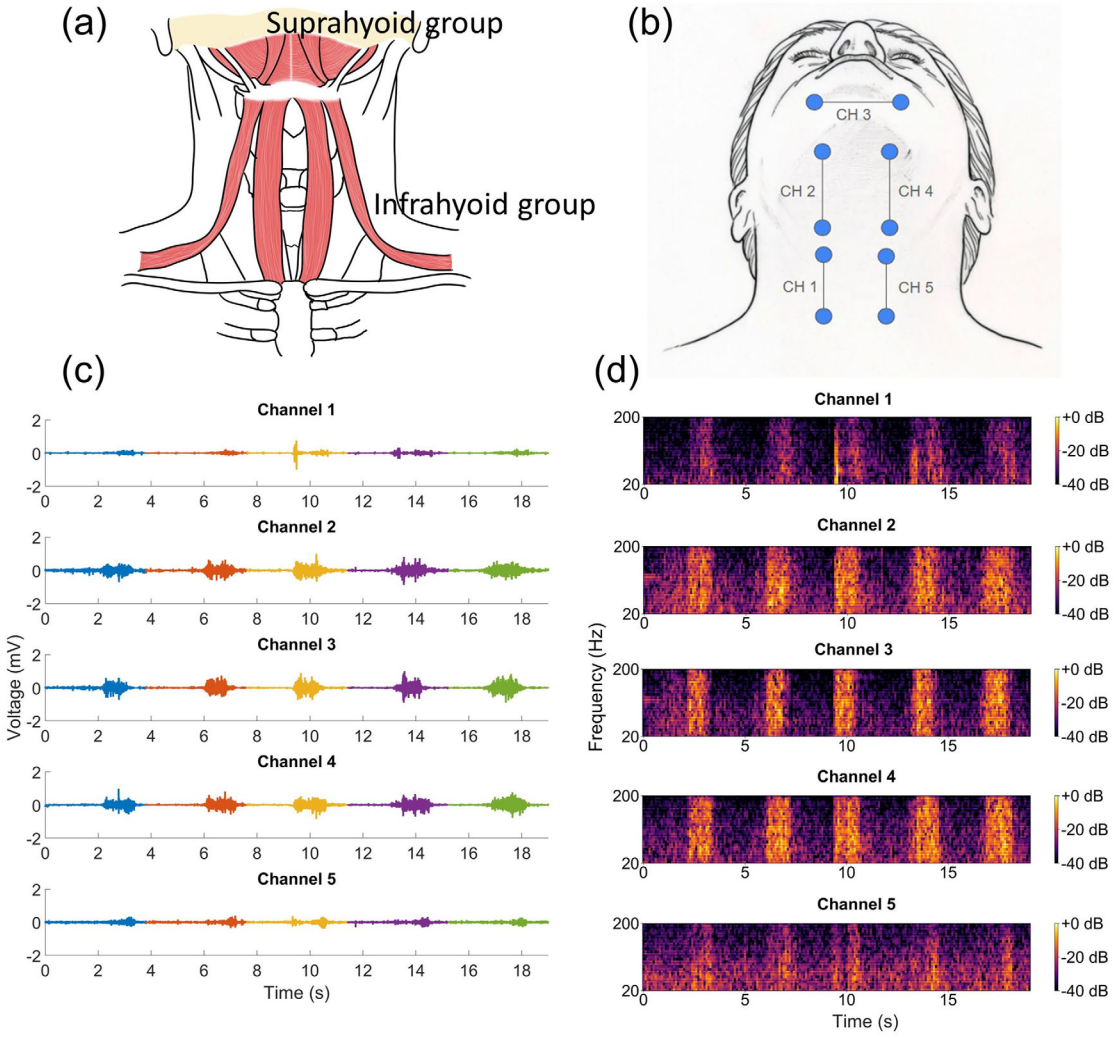

Figure 5. EMG signals associated with the swallowing process. a) Schematics illustrating involved muscle groups during the swallowing process, modified from reference with permission.[58] b) Electrode positions for five pairs/channels of electrodes. c) Collected five-channel EMG signals. Each color means one swallow. d) Mel spectrogram of the collected five-channel EMG signals. When conducting the Fourier Transform to get the Mel spectrogram, the window length and hop length were set to 0.2 and 0.1 s, respectively. The presented signals in (c) and (d) are for dry swallows.

the electrode experienced relatively large resistance variations at the beginning of the cyclic stretching/releasing tests (Figure S3, Supporting Information), and the resistance change was stabilized afterward. The resistance variations were within 6% during the 2000 stretching/releasing cycles, demonstrating the electrode's good electromechanical stability.

As observed in our experiments and the literature, slight resistance variations would not affect EMG sensing performance if the skin-electrode impedance remains stable.[20] As for the long-term use of the IONOGEL, the ionic liquid used in our electrodes (EMIM TFSI) has a very high boiling point (543.6 °C from the datasheet) and extremely low vapor pressure (≈10^{-8} Pa from the datasheet), indicating a negligible evaporation rate. A liquid's evaporation rate within a polymer will generally be lower than the evaporation rate of the same liquid in its pure, unconstrained state.[44] A one-week experiment was conducted to test if the developed IONOGEL can effectively collect EMG data. The electrode was attached to the subject's skin for one week, and EMG signals were collected daily. The results show that the SNRs of EMG signals remain stable throughout the week (Figure S4, Supporting Information), confirming the electrode's reliability for at least one week of continuous use.

2.3. Collection and Preprocessing of the Swallow-Induced EMG Signals

IONOGEL electrodes were applied according to the locations in **Figure 5** to target essential muscle groups involved in the swallowing process.[45] The electrode positions that cover the muscles from the infrahyoid and suprahyoid groups were selected (Figure 5a). This ensures that the collected EMG signal conveys the information highly related to the swallowing process. Channels 2, 3, and 4 monitor voluntary and involuntary muscle movements involved in swallowing while channels 1 and 5 monitor

involuntary movements only (Figure 5b).[45,46] The ground electrode was placed on the collarbone, and all wires were spaced a distance apart to eliminate possible interference or crosstalk from other electrodes.

After the signal collection, a bandpass filter (20 – 200 Hz) and a notch filter (60 Hz) were applied to the raw signal to minimize noises and amplify the muscle signals activated during swallowing. Following this, the filtered signal was segmented to separate signal bursts from background data and noise.[39,47,48] Each segment corresponds to a single swallowing event, extracted by identifying the peaks of the signal (Figure 5c). This approach ensures that the most significant data from each swallowing trial is used for feature extraction during machine learning classification. Then, Mel-frequency cepstral coefficients (MFCC) were extracted as features from the EMG signals and effectively capture the signal's frequency components utilizing a "Mel scale". MFCC features mimic human perception, giving more weight to low frequencies and less to high frequencies.[49,50] It turns out that MFCC is also particularly useful for analyzing muscle activity patterns and identifying subtle variations in EMG signals, especially when dealing with complex muscle movements or differentiating between muscle groups.[51] The MFCC extraction process involves several steps. First, the signals were divided into 0.2 s windows with a 0.1 s overlap. Each window was then transformed into the frequency domain using a Fourier Transform. The resulting spectrum was mapped onto the Mel scale, as shown in Figure 5d. Next, the first 13 (lowest-dimensional) MFCC features were extracted. Finally, MFCC features corresponding to each swallowing event were obtained with the help of the segment results in Figure 5c. Simply put, the MFCC extraction process is similar to frequency feature extraction using the Fourier Transform, with the key difference being that the spectrum is mapped onto the Mel scale. All the processes can be finished using the open-source library 'librosa'.[52]

2.4. Swallowing Classification and Regression using Machine Learning

Following signal pre-processing, MFCC features and corresponding labels for EMG signals were used to train machine learning models for classifying swallow events from collected EMG signals. These events included dry swallows and swallowing 4 different foods – 1 Ritz cracker, 0.5 tsp Yoplait yogurt, 5 mL of water, and 15 mL of water – selected based on their varying viscosities and volumes. Each event was repeated ten times. SVM and ANN algorithms, using fivefold cross-validation, were employed to train the models. Through this validation method, the data was divided randomly into five sets: Four of the sets were used to train the model, and the model was validated using the remaining set. As shown in the confusion matrix (**Figure 6**a,b), the average validation accuracies of SVM classification and ANN classification are 98.0% and 94.0%, respectively. The SVM model slightly outperforms the ANN in distinguishing between different swallow types. Overall, these results demonstrate the great feasibility and effectiveness of the classification models in recognizing various swallowing activities across different food textures and volumes.

In addition to classification, a regression model was developed to predict swallow volumes based on EMG signals, focusing primarily on dry and water swallows. Regression predicts continuous values, such as swallow volumes, rather than categorical labels. Unlike classification, which assigns predefined classes, regression models estimate numerical outputs based on input features, enabling precise measurement of swallowing volumes from EMG signals. The SVM model (Figure 6c) shows a better performance in predicting 5 and 15 mL water swallows than the ANN model (Figure 6d). However, for the prediction of dry swallows, the SVM model shows a larger variation compared to the ANN. Overall, the regression accuracy for SVM and ANN is ±1.17 and ±2.17 mL, respectively, which means SVM has a better performance for the collected data set. ANN is inherently more data-hungry than SVM for regression tasks, requiring larger datasets to achieve comparable accuracy. While ANN's performance could be improved with larger datasets and detailed tuning of hyperparameters, SVM remains preferable for both classification and regression tasks due to its robustness with small-sample and high-dimensional data, enabling data-efficient generalization. While there are different ways to track daily water intake, this study shows an accurate, portable, and unobtrusive way for distinguishing different swallow events enabled by continuous biopotential sensing and machine learning models. The ability to predict swallow events from the collected EMG signals demonstrates the great potential of the developed sensors and models as highly accurate diagnostic tools.

To assess whether symmetrically positioned channels provide complementary information, cross-correlation analysis was performed on the root mean square (RMS) smoothed EMG signals (Figure S5, Supporting Information). Raw EMG signals were considered unsuitable for such analysis because they have rapid baseline-crossing oscillations, which would make the correlation analysis uninformative even between physiologically relevant channels. Results showed a strong cross-correlation between Channels 3 and 4 (Table S4, Supporting Information), consistent with their symmetrical anatomical locations. In contrast, despite their symmetrical location, Channels 1 and 5 showed a weaker correlation, due to their lower signal amplitude and increased susceptibility to noise. **Figure 7** demonstrates the performance of the SVM model for food classification and water volume regression using various combinations of EMG sensor channels. For food classification, reducing the number of channels from 5 to 2 (specifically, with Channels 1 and 4 remaining) decreased overall accuracy by only 4% (98% to 94%, as shown in Figure 7a), demonstrating that a 60% reduction in electrode count has minimal impact on classification performance. The combination of Channels 1 and 4 retained robust accuracy as these electrodes are positioned over the infrahyoid group, which dominates swallowing activation. Other channels (2, 3, 5) provide redundant information to channels 1 and 4. The analysis shows the spatial specificity (attachment positions) of EMG signals, enabling simplified configurations for classification without sacrificing much of the performance. However, for water volume regression (Figure 7b), such reduction in channels has a more pronounced effect. The average prediction error increases by nearly 80% when using only two channels compared to all five, indicating that regression tasks require more data inputs for accurate predictions. Another key piece of information is that the SVM model trained exclusively on Channels 2, 3, and 4 achieved 92% classification accuracy and ±2.00 mL regression error, while adding Channels 1 and 5

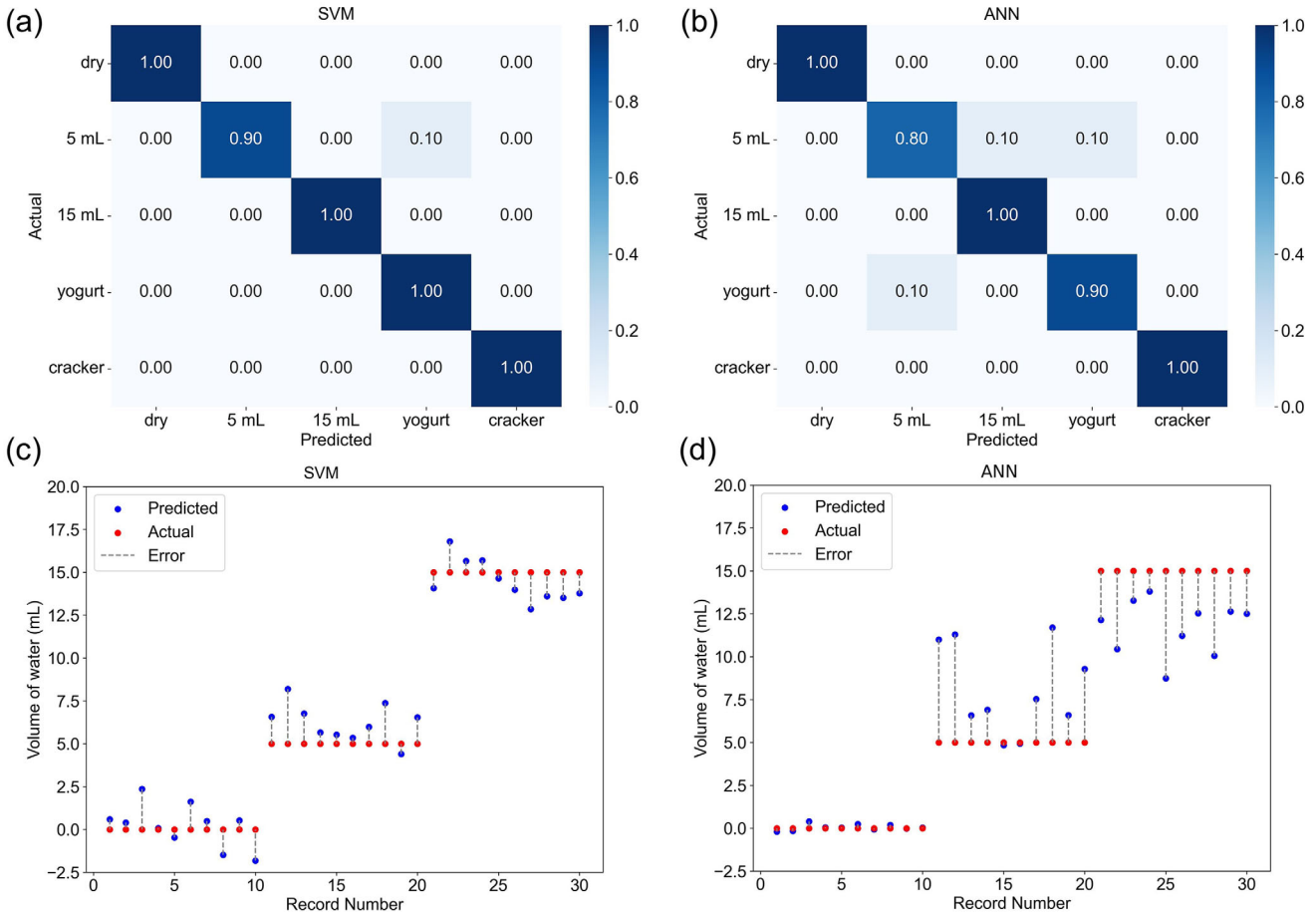

Figure 6. Results for classification and regression models for Subject 1. a,b) Confusion matrices for the classification models using (a) SVM and (b) ANN, respectively. The average accuracy is 98% for SVM and 94% for ANN. c,d) Prediction results for the regression models using (c) SVM and (d) ANN, respectively. Predicted negative values in (c) and (d) were clamped to 0 mL, as negative volumes are non-physical in this context.

improved the accuracy. This implies that despite lower signal amplitudes and potentially higher noise susceptibility, Channels 1 and 5 provide supplementarily useful information for swallow monitoring.

Besides, results from two subjects were compared to further reveal the impact of channel configurations. It should be noted that for both subjects, channel 3 (suprahyoid group) had lower classification accuracy than the infrahyoid channels (1, 2, 4, 5), as shown in Table S5 (Supporting Information). EMG signals from two channels are sufficient for the model to obtain great classification accuracy for both subjects (Table S6, Supporting Information). As for regression tasks (Table S7, Supporting Information), it is crucial to use data from all channels, as fewer channels lead to higher errors. These models are user-dependent, as EMG signal patterns vary significantly between individuals due to anatomical and physiological differences. The user-dependency is also found in our prior work on biopotential-based speech recognition systems.[39,48] These findings have important implications for the design of wearable swallowing monitoring devices that allow for simplified configurations in food classification and volume estimation.

To develop a more compact system, Table S8 (Supporting Information) shows the recommended electrode configurations for different numbers of channels based on Subject 1. If based on Subject 2, the channel selection results are very similar. While the SVM model maintains high classification accuracy even with reduced channels (Figure S6, Supporting Information), the regression model requires more channels for precise predictions, as reducing the number of channels significantly increases regression error (Figure S7, Supporting Information). Therefore, minimizing channels is not recommended for regression tasks.

3. Conclusion

In conclusion, the reported materials, electrode design, fabrication processes, and machine learning models provide a mechanically and visually unobtrusive solution for monitoring EMG signals involved in swallowing. The skin-conformal and comfortable electrodes ensure that users can seamlessly integrate them into daily activities without discomfort or disruption. The simple aqueous fabrication process and 3D conductivity of the electrodes facilitate the devices' integration with external components, offering versatility for healthcare applications. Moreover, the proof-of-concept demonstrations illustrate the system's potential as both a diagnostic and rehabilitation tool. The classification model successfully differentiates between five distinct swallowed food

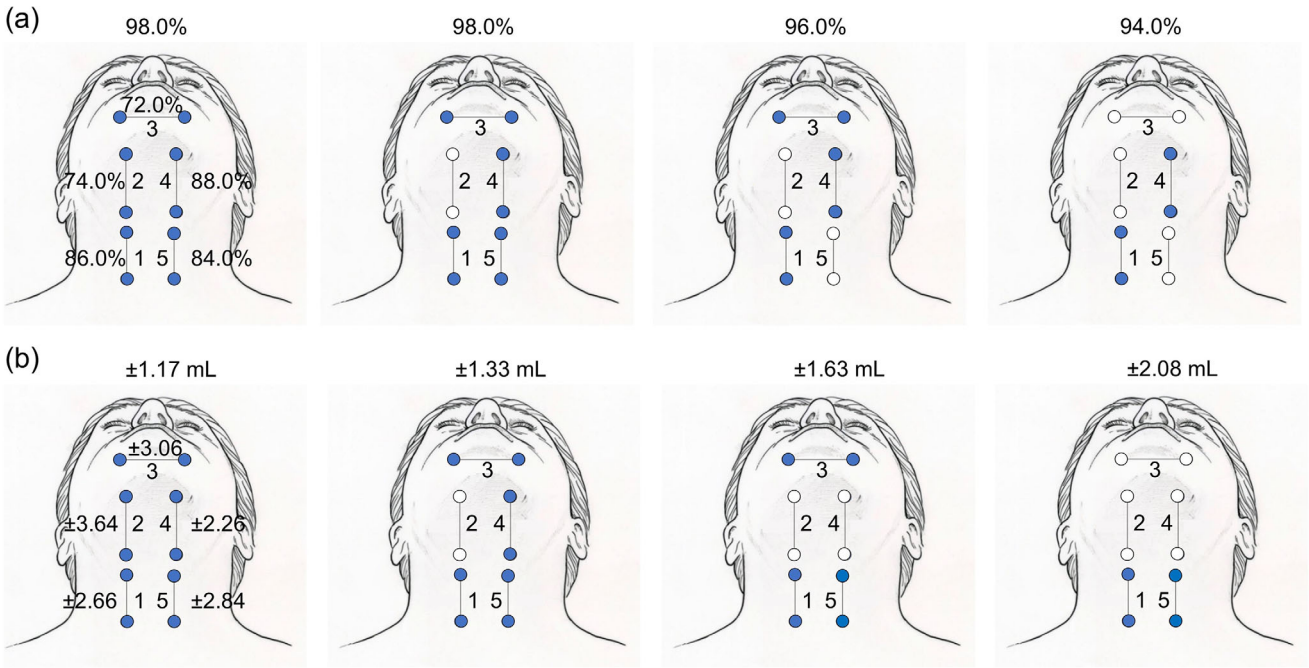

Figure 7. Recognition results for different combinations of channels by the SVM model. a) Accuracies for the food classifications. b) Accuracies for swallowing water volume regressions. The first configuration in each subplot used all five channels, and the accuracy of each channel alone is marked on the schematic.

textures and volumes, reflecting varying muscle strengths that could be critical for assessing patients with swallowing disorders. Additionally, the regression model accurately estimates fluid intake per swallow, providing an objective and quantitative assessment of swallowing performance, which is significant for evaluating dysphagia risk and informing clinical decisions. These innovations not only advance the field of unobtrusive EMG monitoring but also open new avenues for patient-specific diagnostics and rehabilitation in the management of swallowing disorders.

4. Experimental Section

Materials: WPU aqueous dispersion (Bondthane UD-410, 35% dispersion) was purchased from Bond Polymers International. PEDOT:PSS (mean particle size: ≈30nm) aqueous solution was purchased from MSE Supplies. EMIM TFSI (≥98% purity) and DMSO (≥99.9% purity) were purchased from Sigma–Aldrich. All chemicals were used as received without any further purification.

Fabrication of Electrodes: To prepare the electrodes, WPU was first mixed with PEDOT:PSS and DMSO (half the weight of PEDOT:PSS) solutions in a vortex mixer (Thinky, AR-100) at 1000 rpm for ≈1 min. Since the aqueous dispersion form of PEDOT:PSS was used, DMSO served to facilitate the homogeneous dispersion of PEDOT:PSS throughout the polymer. After the solution was thoroughly mixed, EMIM TFSI was added to the solution and stirred at 1000 rpm for 1 min until a homogenous cloudy solution was obtained. A small amount of deionized water was then added to the solution to decrease the viscosity of the solution and allow for easier handling when pouring into the mold. After distributing the solution on the glass substrate, it was cured at 70 °C for 4 h. After the solution was cured, the electrode was patterned into the desired shape using a utility knife. For different samples, the weight ratios of WPU to EMIM TFSI in each sample were 60:40 (IONOGEL-40), 70:30 (IONOGEL-30), or 80:20 (IONOGEL-20), respectively. The weight ratios of PEDOT:PSS to the WPU and EMIM TFSI mixture were 2%, 5%, or 7.5%, respectively.

Characterization: The stress–strain curves of IONOGEL electrodes were measured using a tensile stage (MTS, 858 Mini Bionix II) at a speed of 5 mm min^{-1} according to the ASTM D412 standard.[53] The load cell of the tensile stage has a resolution of 0.001 N. The engineering stress was adopted for the stress calculation. The adhesion force was also tested using the same tensile stage and the same parameters. The electrode was attached to the pig skin and the adhesion force was measured by the load cell during the delamination between the electrode and the pig skin. The adhesion force was calculated by dividing the maximum stable force by the electrode width.[54]

To assess the electrode-skin impedance, the electrodes were applied to the forearm skin, spaced 8 cm apart. To ensure repeatability between measurements, the electrodes were placed in identical locations on the forearm for each impedance test. The impedance between the electrodes was measured using an impedance analyzer (Keysight, E4990A). Transmittance of the electrodes was evaluated with UV–vis Spectroscopy (Thermal Scientific, Genesys 30) across wavelengths from 400 to 700 nm. Each sample was attached to a glass microscope slide and placed inside the UV–vis analyzer in such a way that all outgoing light passed onto the microscope slide. The analyzer was calibrated to zero with a blank microscope slide.

An electrochemical impedance spectroscopy (EIS) experiment was performed to evaluate the ionic conductivity of the electrode when no PEDOT:PSS was added in. Following the standard EIS measurement protocol for ionic materials,[55] AC signals with frequencies ranging from 0.1 Hz to 7 MHz were applied using a potentiostat (BioLogic, VSP-300). The resulting Nyquist plot was used to calculate the ionic conductivity of the developed ionic materials (Figure S2, Supporting Information). Briefly, after getting the Nyquist plot, the ionic conductivity can be calculated by the equation: $\sigma = L/(R_b \cdot A)$.[55] L, R_b, and A are the thickness, bulk resistance, and area of ionic material, respectively.

Since the PEDOT:PSS is both electrically and ionically conductive,[56] the electrodes exhibit electrical conductivity with the addition of PEDOT:PSS. The conductivity of the electrode with PEDOT:PSS was evaluated with a Digital Multimeter (Keysight, 34470A). Each sample had a cross-sectional area of 1 cm by 0.03 cm. The resistance was measured using the multimeter, and the conductivity of the sample was calculated

using the equation $\sigma = L/(R{\cdot}A)$. where L, R, and A are the length, resistance, and cross-sectional area of the sample, respectively. After the conductivity measurement, the cyclic test of the resistance changes under strain for the electrode was conducted using a tensile stage (MTS, 858 Mini Bionix II). The maximum tensile strain was set to 15%.

EMG Signal Collection: This study was approved by the Institutional Review Board (IRB2024-00240), the institutional ethics committee at Stony Brook University, ensuring compliance with ethical standards for human subject research. The EMG signals were extracted using bio amplifiers (AD Instruments, Octal BioAmp) and a data acquisition system (AD Instruments, PowerLab 8/30) through the LabChart Pro software at a sampling frequency of 1 kHz. For analysis and visualization, a bandpass filter with a low cutoff frequency of 20 Hz and a high cutoff frequency of 200 Hz was applied according to the standard of the International Society of Electrophysiology and Kinesiology.[57] In addition, to minimize background noise, a 60 Hz notch filter was applied using the LabChart software. The *SNR* was calculated by the following equation:

$$SNR_{dB} = 20\log_{10}\left(\frac{A_{signal}}{A_{noise}}\right) \quad (1)$$

where A_{signal} is the root mean square of the EMG signals and A_{noise} is the root mean square of the noise. Signals acquired when the subject was not actively flexing muscles were considered as noise.

Model Training: For the SVM classification model, a grid-search cross-validation was conducted to optimize hyperparameters, including the regularization parameter C, kernel coefficient γ, and kernel type. The radial basis function (RBF) kernel was selected due to its ability to model nonlinear decision boundaries in the high-dimensional MFCC feature space. For the ANN classification model, hyperparameters such as learning rate, batch size, and dropout rate were tuned via the fivefold cross-validation to improve accuracy and prevent overfitting. The Adam optimizer and ReLU activation allow the network to learn discriminative spectral-temporal patterns in MFCC features. Similar to the classification model, a support vector regressor (SVR) with RBF kernel was optimized for the SVM model, focusing on parameters C and ϵ (error tolerance) to minimize volume prediction errors. As for the ANN, a separate regression-focused architecture was trained using mean absolute error (MAE) loss, with hyperparameters adjusted to prioritize a smooth prediction of continuous volumes.

Statistical Analysis: Fivefold cross-validation was utilized for SVM and ANN models, achieving classification accuracies of 98.0% (SVM) and 94.0% (ANN) across ten trials per swallow event (five food types, n = 10/event). Regression errors were ±1.17 mL (SVM) and ±2.17 mL (ANN) for the three liquid volumes used in the swallow test. Cross-correlation analysis revealed strong correlations between symmetrical channels (e.g., Channels 3 and 4). Models were optimized via grid-search (SVM) and Adam optimizer (ANN), with analyses performed using Python (scikit-learn, TensorFlow, librosa).

Supporting Information

Supporting Information is available from the Wiley Online Library or from the author.

Acknowledgements

P.D. and J.I. contributed equally to this work. This material is based upon work supported by the National Science Foundation under Award No. ECCS-2335863. The authors express the gratitude to Professor Xinwei Mao and Research Scientist Dr. Mian Wang, from the Department of Civil Engineering at Stony Brook University for their support with the UV–vis testing system. The authors sincerely thank Professor Lifeng Wang and his Ph.D. student, Xihang Jiang, from the Department of Mechanical Engineering at Stony Brook University for their assistance with tensile testing. Additionally, the authors would like to thank Professor Yu-chen Karen Chen-Wiegart and her Ph.D. student Varun Kankanallu from the Department of Materials Science and Chemical Engineering at Stony Brook University for assisting with EIS experiments.

Conflict of Interest

The authors declare no conflict of interest.

Data Availability Statement

The data that support the findings of this study are available from the corresponding author upon reasonable request.

Keywords

biopotential electrodes, electromyography, machine learning, swallow monitoring

Received: February 2, 2025
Revised: April 8, 2025
Published online:

[1] J. A. Logemann, *Curr. Opin. Otolaryngol. Head Neck Surg.* **1998**, *6*, 395.
[2] M. Cabre, M. Serra-Prat, E. Palomera, J. Almirall, R. Pallares, P. Clave, *Age Ageing* **2010**, *39*, 39.
[3] K. Tjaden, *Top. Geriatr. Rehabil.* **2008**, *24*, 115.
[4] H. Siebens, E. Trupe, A. Siebens, F. Cook, S. Anshen, R. Hanauer, G. Oster, *J. Am. Geriatr. Soc.* **1986**, *34*, 192.
[5] S. Singh, S. Hamdy, *Postgrad. Med. J.* **2006**, *82*, 383.
[6] N. Miller, E. Noble, D. Jones, D. Burn, *Age Ageing* **2006**, *35*, 614.
[7] B. J. Martin, M. M. Corlew, H. Wood, D. Olson, L. A. Golopol, M. Wingo, N. Kirmani, *Dysphagia* **1994**, *9*, 1.
[8] L. F. Giraldo-Cadavid, L. R. Leal-Leano, G. A. Leon-Basantes, A. R. Bastidas, R. Garcia, S. Ovalle, J. E. Abondano-Garavito, *Laryngoscope* **2017**, *127*, 2002.
[9] H. R. Ingleby, H. S. Bonilha, C. M. Steele, *Dysphagia* **2023**, *38*, 517.
[10] T. Rafeedi, A. Abdal, B. Polat, K. A. Hutcheson, E. H. Shinn, D. J. Lipomi, *Npj Flex. Electron.* **2023**, *7*, 52.
[11] D. Zhang, Z. Chen, L. Xiao, B. Zhu, R. Wu, C. Ou, Y. Ma, L. Xie, H. Jiang, *Microsyst. Nanoeng.* **2023**, *9*, 115.
[12] B. Shin, S. H. Lee, K. Kwon, Y. J. Lee, N. Crispe, S. Y. Ahn, S. Shelly, N. Sundholm, A. Tkaczuk, M. K. Yeo, H. J. Choo, W. H. Yeo, *Adv. Sci.* **2024**, *11*, 2404211.
[13] M. K. Kim, C. Kantarcigil, B. Kim, R. K. Baruah, S. Maity, Y. Park, K. Kim, S. Lee, J. B. Malandraki, S. Avlani, A. Smith, S. Sen, M. A. Alam, G. Malandraki, C. H. Lee, *Sci. Adv.* **2019**, *5*, aay3210.
[14] A. Cesareo, E. Biffi, D. Cuesta-Frau, M. G. D'Angelo, A. Aliverti, *Med. Biol. Eng. Comput.* **2020**, *58*, 785.
[15] Y. J. Kang, *Signals* **2024**, *5*, 516.
[16] S. K. Archer, C. H. Smith, D. J. Newham, *Dysphagia* **2021**, *36*, 281.
[17] M. Vaiman, *Head Face Med.* **2007**, *3*, 26.
[18] B. N. Krekeler, C. K. Broadfoot, S. Johnson, N. P. Connor, N. Rogus-Pulia, *Dysphagia* **2018**, *33*, 173.
[19] C. Malvuccio, E. N. Kamavuako, *Sensors* **2022**, *22*, 3380.
[20] S. Yao, W. Zhou, R. Hinson, P. Dong, S. Wu, J. Ives, X. Hu, H. Huang, Y. Zhu, *Adv. Mater. Technol.* **2022**, *7*, 2101637.
[21] W. Zhou, S. Yao, H. Wang, Q. Du, Y. Ma, Y. Zhu, *ACS Nano* **2020**, *14*, 5798.
[22] Y. Fu, J. Zhao, Y. Dong, X. Wang, *Sensors* **2020**, *20*, 3651.

[23] M. Zhu, B. Yu, W. Yang, Y. Jiang, L. Lu, Z. Huang, S. Chen, G. Li, *Biomed. Eng. Online* **2017**, *16*, 133.
[24] H. Kim, E. Kim, C. Choi, W. H. Yeo, *Micromachines* **2022**, *13*, 629.
[25] L. Hu, P. L. Chee, S. Sugiarto, Y. Yu, C. Shi, R. Yan, Z. Yao, X. Shi, J. Zhi, D. Kai, H. D. Yu, W. Huang, *Adv. Mater.* **2023**, *35*, 2205326.
[26] D. Xu, X. Meng, S. Liu, J. Poisson, P. Vana, K. Zhang, *Nat. Commun.* **2024**, *15*, 6886.
[27] H. He, *J. Ouyang, Acc. Mater. Res.* **2020**, *1*, 146.
[28] E. H. Houssein, M. E. Hosney, M. M. Emam, E. M. G. Younis, A. A. Ali, W. M. Mohamed, *Artif. Intell. Rev.* **2023**, *56*, 2599.
[29] L. R. Quitadamo, F. Cavrini, L. Sbernini, F. Riillo, L. Bianchi, S. Seri, G. Saggio, *J. Neural Eng.* **2017**, *14*, 011001.
[30] R. Singla, B. Chambayil, A. Khosla, J. Santosh, *J. Biomed. Sci. Engineer.* **2011**, *04*, 62.
[31] R. M. Singh, V. Ahlawat, S. Chatterji, A. Kumar, *J. Interdiscip. Math.* **2020**, *23*, 153.
[32] H. Bhavsar, M. H. Panchal, *IJARCET.* **2012**, *1*, 185.
[33] J. Cervantes, F. Garcia-Lamont, L. Rodríguez-Mazahua, A. Lopez, *Neurocomputing* **2020**, *408*, 189.
[34] A. Alwosheel, S. van Cranenburgh, C. G. Chorus, *J. Choice Model.* **2018**, *28*, 167.
[35] D. A. Gabriel, *Med. Eng. Phys.* **2011**, *33*, 1079.
[36] A. Akinin, A. Paul, J. Wang, A. Buccino, G. Cauwenberghs, *Neural. Eng.* **2020**, 65.
[37] J. P. do Vale Madeiro, P. C. Cortez, J. M. da Silva Monteiro Filho, P. R. F. Rodrigues, in *Developments and Applications for ECG Signal Processing*, Elsevier, Netherlands **2019**, Ch. 3.
[38] E. J. Shin, S. M. Choi, *Adv. Exp. Med. Biol.* **2018**, *1077*, 251.
[39] P. Dong, Y. Song, S. Yu, Z. Zhang, S. K. Mallipattu, P. M. Djuric, S. Yao, *Small* **2023**, *19*, 2205058.
[40] M. Kim, H. K. Um, H. Choi, J. S. Lee, J. Kim, K. Kim, E. Noh, M. W. Han, H. W. Lee, W. I. Choi, S. H. Lee, J. R. Lee, B. H. Lee, *Adv. Electron. Mater.* **2023**, *9*, 2300075.
[41] Y. Li, Y. Pang, L. Wang, Q. Li, B. Liu, J. Li, S. Liu, Q. Zhao, *Adv. Mater.* **2024**, *36*, 2310973.
[42] L. S. de Vasconcelos, Y. Yan, P. Maharjan, S. Kumar, M. Zhang, B. Yao, H. Li, S. Duan, E. Li, E. Williams, *Cell Biomater.* **2025**, *1*, 100004.
[43] W. Yang, R. He, R. Goossens, T. Huysmans, *Appl. Ergon.* **2023**, *106*, 103916.
[44] N. Hosoya, K. Nishiguchi, H. Saito, S. Maeda, *J. Chem. Eng.* **2022**, *444*, 136506.
[45] Enovis, VitalStim Therapy Electrode Placement With Neck Muscles, https://enovis.com/sites/default/files/vitalstim/VitalStim_Therapy_Electrode_Placement_On_The_Neck.pdf, (accessed: July 2024).
[46] R. K. Goyal, H. Mashimo, Physiology of oral, pharyngeal, and esophageal motility, https://www.nature.com/gimo/contents/pt1/full/gimo1.html, (accessed: July 2024).
[47] P. Dong, Y. Li, S. Chen, J. T. Grafstein, I. Khan, S. Yao, *Mater. Horiz.* **2023**, *10*, 5607.
[48] P. Dong, S. Tian, S. Chen, Y. Li, S. Li, M. Zheng, S. Yao, *Adv. Mater. Technol.* **2025**, *10*, 2400990.
[49] M. Xu, L. Y. Duan, J. Cai, L. T. Chia, C. S. Xu, Q. Tian, *Proceedings* **2004**, *3333*, 566.
[50] Y. Li, A. Parsan, B. Wang, P. Dong, S. Yao, R. Qin, *Eng. Appl. Artif. Intell.* **2023**, *117*, 105597.
[51] A. C. Tsai, J. J. Luh, T. T. Lin, *Expert Syst. Appl.* **2015**, *42*, 3327.
[52] Librosa Development Team, https://librosa.org/doc/latest/feature.html, (accessed: July 2024).
[53] S. V. Sheets, P. from Products, *Annu. B. ASTM Stand* **2012**, *1*, 1.
[54] L. Zhang, K. S. Kumar, H. He, C. J. Cai, X. He, H. Gao, S. Yue, C. Li, R. C. Seet, H. Ren, J. Ouyang, *Nat. Commun.* **2020**, *11*, 4683.
[55] Y. Ding, *Z. Zheng, Matter* **2022**, *5*, 2570.
[56] J. Rivnay, S. Inal, B. A. Collins, M. Sessolo, E. Stavrinidou, X. Strakosas, C. Tassone, D. M. Delongchamp, G. G. Malliaras, *Nat. Commun.* **2016**, *7*, 11287.
[57] R. Merletti, P. Di Torino, *J. Electromyogr. Kinesiol.* **1999**, *9*, 3.
[58] P. C. W. Fung, R. K. C. Kong, *Chin. Med.* **2020**, *11*, 31.